

Density functional theory calculations on entire proteins for free energies of binding: Application to a model polar binding site

Stephen J. Fox,¹ Jacek Dziedzic,^{1,2} Thomas Fox,³ Christofer S. Tautermann,³ and Chris-Kriton Skylaris^{1*}

¹ School of Chemistry, University of Southampton, Southampton, Hampshire SO17 1BJ, United Kingdom

² Faculty of Applied Physics and Mathematics, Gdansk University of Technology, Gdansk, Poland

³ Department for Lead Identification and Optimization Support, Boehringer Ingelheim Pharma GmbH & Co KG, 88397 Biberach, Germany

ABSTRACT

In drug optimization calculations, the molecular mechanics Poisson-Boltzmann surface area (MM-PBSA) method can be used to compute free energies of binding of ligands to proteins. The method involves the evaluation of the energy of configurations in an implicit solvent model. One source of errors is the force field used, which can potentially lead to large errors due to the restrictions in accuracy imposed by its empirical nature. To assess the effect of the force field on the calculation of binding energies, in this article we use large-scale density functional theory (DFT) calculations as an alternative method to evaluate the energies of the configurations in a “QM-PBSA” approach. Our DFT calculations are performed with a near-complete basis set and a minimal parameter implicit solvent model, within the self-consistent calculation, using the ONETEP program on protein–ligand complexes containing more than 2600 atoms. We apply this approach to the T4-lysozyme double mutant L99A/M102Q protein, which is a well-studied model of a polar binding site, using a set of eight small aromatic ligands. We observe that there is very good correlation between the MM and QM binding energies in vacuum but less so in the solvent. The relative binding free energies from DFT are more accurate than the ones from the MM calculations, and give markedly better agreement with experiment for six of the eight ligands. Furthermore, in contrast to MM-PBSA, QM-PBSA is able to correctly predict a nonbinder.

Proteins 2014; 82:3335–3346.
© 2014 Wiley Periodicals, Inc.

Key words: free energies of binding; protein–ligand interactions; DFT; large-scale DFT; ONETEP; QM-PBSA; T4-lysozyme L99A/M102Q.

INTRODUCTION

Advances in computational chemistry and biochemistry are directed toward more accurate descriptions of protein–ligand binding energies, which are essential for the prediction of ligand binding affinities, a long-standing goal in the field of computational drug design.^{1,2} Many methods have been developed to tackle this problem, ranging from theoretically rigorous approaches such as free energy perturbation^{3,4} and thermodynamic integration (TI),⁵ to cheap and fast scoring methods⁶ commonly used for docking calculations.

A method of medium computational effort is the molecular mechanics Poisson-Boltzmann surface area (MM-PBSA) approach.⁷ This approach combines molecular dynamics (MD) simulations and continuum solvation models to estimate protein–ligand binding free

energies. A significant source of error in MM-PBSA can be the accuracy of the interaction energies computed for each snapshot, as this accuracy depends on the selected force field. Force fields have limitations due to their empirical parametrization, which can be unreliable for novel compounds significantly different from those present in the fitting set. Another limitation of most force

Grant sponsor: Engineering and Physical Sciences Research Council (EPSRC); Grant number: EP/J015059/1 (to JD); Grant sponsors: Polish National Science Centre and the Ministry of Science and Higher Education; Grant numbers: N519 577838 and IP2012 043972; Grant sponsor: UCKP consortium (EPSRC; for access to national supercomputers); Grant number: EP/K013556/1.

*Correspondence to: Chris-Kriton Skylaris, School of Chemistry, University of Southampton, Southampton, Hampshire SO17 1BJ, United Kingdom.
E-mail: c.skylaris@soton.ac.uk

Received 17 June 2014; Revised 6 August 2014; Accepted 31 August 2014
Published online 11 September 2014 in Wiley Online Library (wileyonlinelibrary.com). DOI: 10.1002/prot.24686

fields is their inability to explicitly describe electronic polarization and charge transfer. To investigate the effect of these force field-based limitations, in this work we replace the MM energy with a first-principles quantum mechanical (QM) energy evaluated for the entire system, to perform QM-PBSA. For the QM calculations we use the linear-scaling density functional theory (DFT) program ONETEP.⁸ In a previous article,⁹ we investigated the numerical parameters of the implicit solvation model within ONETEP,¹⁰ using as a test system the T4 lysozyme double mutant Leu99Ala/Met102Gln¹¹ (or L99A/M102Q). In this study we will also be using T4 lysozyme L99A/M102Q to calculate QM-PBSA-based relative free energies of binding for various ligands.

There has been a great deal of research into protein stability, folding and design by looking at mutations of the lysozyme from the bacteriophage T4.^{12,13} Two well-studied mutants of T4 lysozyme are Leu99Ala (L99A)^{12,14–16} and L99A/M102Q.¹¹ These mutations create a small buried apolar and polar cavity respectively, which are capable of encapsulating small aromatic ligands. These T4 lysozyme mutants have been used to compare and validate binding free energy methods^{14,17–21} and to develop docking procedures.^{11,22,23} The relative simplicity of the T4 lysozyme mutants and their small size make them attractive for validating computational methods. Coupled with the abundance of literature, this makes T4 lysozyme L99A/M102Q a good choice for a benchmark of QM-PBSA calculations.

In this study we are comparing the free energy of binding between the conventional MM-PBSA approach and our QM-PBSA approach on eight ligands bound to the T4 lysozyme double mutant L99A/M102Q. These ligands were chosen as they comprise a variety of chemical and physical properties (polarity, inclusion of halides, size and nonbinders). Methods section describes the MM-PBSA method, some of its most common variants, ONETEP and our solvation model, QM-PBSA and our simulation protocols and parameters. In Results and discussion section, we present and discuss our calculation results and, we finish with conclusions in Conclusions section.

METHODS

MM-PBSA and QM-PBSA

Ligand binding affinity is calculated as

$$\Delta G_{\text{bind}} = G_{\text{complex}} - G_{\text{receptor}} - G_{\text{ligand}}. \quad (1)$$

MM-PBSA⁷ is a method for computationally predicting ligand binding affinity. The approach is based on the postprocessing of a molecular dynamics trajectory, typically run in explicit solvent and counterions in a periodic box. The free energy of binding is estimated by extract-

ing a representative structural ensemble of “snapshots” from the trajectory. Solvent molecules and counterions are removed, then MM is used to calculate the gas phase interaction energy and a continuum solvent model (PBSA) is used to calculate the solvation energies. The free energy of binding is then obtained as the average over the ensemble of structures:

$$\Delta G = \langle \Delta E^{\text{MM}} \rangle + \langle \Delta G_{\text{PBSA}} \rangle - T \langle \Delta S^{\text{MM}} \rangle, \quad (2)$$

where $\langle \Delta E^{\text{MM}} \rangle$ is the interaction energy in vacuum, $\langle \Delta G_{\text{PBSA}} \rangle$ is the solvation energy, and $\langle \Delta S^{\text{MM}} \rangle$ is the solute entropy, which can be obtained using normal mode analysis. By using a continuum solvent model, the problem is simplified since we are implicitly integrating out all the solvent coordinates, which results in more rapid convergence with the number of snapshots.

The straightforward way to calculate the binding free energy is the three-trajectory approach, where separate simulations are carried out for the complex, receptor and ligand. However, it has been found that the one-trajectory approach, where only the complex simulation is run, and receptor and ligand configurations are extracted from the complex geometries, is more accurate due to error cancellation.²⁴ It is also 2–3 times faster, since the most computationally demanding part is the MD simulations. However, this approach assumes that there are no conformational changes to the ligand or receptor upon binding. Furthermore, when using the single trajectory approach, $\langle E^{\text{MM}} \rangle$ is the difference in nonbonded terms only, since all bonded terms will cancel.

Calculation of the entropy in a consistent and accurate manner is challenging. This makes calculation of the absolute binding free energies difficult. An approximation that is often used is that entropy change is assumed to be comparable for similar ligands, and hence cancels when considering relative free energies of binding. Although this may seem a poor assumption, calculating the entropy of the ligand from structures taken from the complex trajectory may well be an equally poor simplification; since the ligand would be expected to have many more degrees of freedom when free in solution. The relative free energy is calculated as

$$\Delta \Delta G_{A \rightarrow B} = \Delta \langle \Delta E^{\text{MM}} \rangle_{A \rightarrow B} + \Delta \langle \Delta G_{\text{solv}} \rangle_{A \rightarrow B}. \quad (3)$$

A significant source of error in MM-PBSA can be the accuracy of the interaction energies computed for each snapshot, as this accuracy depends on the parametrization and transferability of the selected force field. Apart from the obvious approach of using more advanced force fields, a related direction for improvement is to replace either part or all of the force field description by a quantum description of the system. This would be expected to be more accurate and transferable due to explicitly accounting for the electronic effects, which are the source of all the interactions.

Kaukonen *et al.*²⁵ presented a QM/MM-PBSA approach and compared it to MM-PBSA for the purpose of studying reactions in proteins. The aim was to study the stability of two states with a shared proton. The QM calculations were performed with DFT using the BP86 exchange-correlation functional with a 6–31G* basis set and DZP for metal ions for one system, and the B3LYP functional for another system using the same basis sets. This method showed improved results for the proton transfer and was in good agreement with more rigorous approaches (QTCP²⁶) with median absolute deviations (MADs) of 4–22 kJ/mol. However, the QM region was quite small, comprising 46 atoms while the MM part comprised 12,132 atoms.

Wang and Wong²⁷ used the SIESTA DFT code²⁸ combined with the implicit solvation model in the UHBD software²⁹ in a QM/MM-PBSA approach. The only differences between the ligands in the pocket was a single chemical functional group, with all common atoms being in identical positions. This was done to improve the odds of cancellation of systematic errors when comparing binding free energies. Relaxed structures were generated in three different ways. The first was geometry optimized with SIESTA and the second and third in a QM/MM approach with the ONIOM method in GAUSSIAN03.³⁰ However, no protein configurational sampling was performed. Wang *et al.* used a fixed geometry (single structure) approximation, where only minimized crystal structures are used.

Diaz *et al.*³¹ replaced $\Delta\langle\Delta E^{\text{MM}}\rangle$ with energies from linear-scaling semiempirical QM calculations on an ensemble of structures from a classical MD simulation in a QM-PBSA type model. Prior to the single-point energy calculations, QM/MM geometry optimizations of a subsystem of the enzyme were performed, keeping the rest of the enzyme fixed. Single point energy calculations were performed with AM1 and PM3 using the divide and conquer (D&C) approach on the subsystem of the enzyme. The DivCon99³² program was used to perform the D&C calculations. Diaz *et al.* found that the resulting QM/MM geometry-optimized structures were similar to the MD representations generated from the force fields, and using semiempirical QM D&C gave comparable relative binding free energies to MM-PBSA. However, this uses an empirical method and suffers from some of the same transferability problems as force fields.

Cole *et al.*³³ have recently extended the MM-PBSA approach to a full QM-PBSA approach, with sampling of protein motion, where the calculation of the interaction energies in vacuum by the force field is replaced by DFT calculations on the entire molecule for an ensemble of snapshots taken from an MD simulation. The energy of each snapshot is obtained as $E^{\text{QM}} = E_{\text{DFT}} + E_{\text{disp}}$, where E_{disp} is the dispersion correction³⁴ to the total DFT energy, E_{DFT} . In previous work,^{33,35} the free energy of solvation in the QM calculation, $G_{\text{solv}}^{\text{QM}}$ was obtained by

scaling the classical solvation energy by the QM electrostatic energy, giving the free energy of binding as

$$\Delta G_{\text{tot}} = \langle\Delta E^{\text{QM}}\rangle + \langle\Delta G_{\text{PB}}\left(\frac{\Delta E_{\text{DFT}}}{\Delta E_{\text{EL}}}\right) + \Delta G_{\text{SA}}\rangle \quad (4)$$

$$= \langle\Delta E^{\text{QM}}\rangle + \langle\Delta G_{\text{solv}}^{\text{QM}}\rangle, \quad (5)$$

where ΔE_{EL} is the electrostatic contribution to the binding energy from the MM calculation, ΔG_{PB} is the polar term from the solvation energy and ΔG_{SA} is the nonpolar term. The first application of QM-PBSA with ONETEP has been on protein–protein interactions.³³ The results obtained were in good agreement with MM-PBSA, most likely because the force field employed has been extensively and carefully parameterized for protein systems and improved over a number of years. This was applied to a model of a host-guest system,³⁵ where the force fields are much more general and harder to parameterize. Here a significant improvement was seen over MM-PBSA for relative binding free energies. However, this does not calculate the QM solvation energy in the QM calculation, and as such is susceptible to the errors in the computed MM solvation energy.

In this work we are presenting the first QM-PBSA study of a protein–ligand system where the entire protein of 2602 atoms has been described by DFT calculations. These calculations have been performed with ONETEP, and in contrast to our previous QM-PBSA studies, the solvation free energy has been computed within ONETEP with a newly implemented self-consistent minimal parameter implicit solvation model.¹⁰

The ONETEP approach

The ONETEP⁸ program is a linear-scaling DFT code that has been developed for use on parallel computers.³⁶ ONETEP combines linear scaling with accuracy comparable to conventional cubic-scaling plane-wave methods, which provide an unbiased and systematically improvable approach to DFT calculations. Its novel and highly efficient algorithms allow calculations on systems containing tens of thousands of atoms.³⁷ ONETEP is based on a reformulation of DFT in terms of the one-particle density matrix. The density matrix in terms of Kohn–Sham orbitals is

$$\rho(\mathbf{r}, \mathbf{r}') = \sum_{n=0}^{\infty} f_n \psi_n(\mathbf{r}) \psi_n^*(\mathbf{r}'), \quad (6)$$

where f_n is the occupancy and $\psi_n(\mathbf{r})$ are the Kohn–Sham orbitals. In ONETEP the density matrix is represented as

$$\rho(\mathbf{r}, \mathbf{r}') = \sum_{\alpha} \sum_{\beta} \phi_{\alpha}(\mathbf{r}) K^{\alpha\beta} \phi_{\beta}^*(\mathbf{r}'), \quad (7)$$

where $\phi_{\alpha}(\mathbf{r})$ are localized nonorthogonal generalized Wannier functions (NGWFs)³⁸ and $K^{\alpha\beta}$, which is called

the density kernel, is the representation of f_n in the duals of these functions. Linear scaling is achieved by truncation of the density kernel, which decays exponentially for materials with a band gap, and by enforcing strict localization of the NGWFs onto atomic regions. In ONETEP, as well as optimizing the density kernel, the NGWFs are also optimized, subject to a localization constraint. Optimizing the NGWFs *in situ* allows for a minimum number of NGWFs to be used whilst still achieving plane wave accuracy. The NGWFs are expanded in a basis set of periodic sinc (psinc) functions,³⁹ which are equivalent to a plane-wave basis as they are related by a unitary transformation. Using a plane wave basis set allows the accuracy to be improved by varying a single parameter, equivalent to the kinetic energy cutoff in conventional plane-wave DFT codes. The psinc basis set provides a uniform description of space, meaning that ONETEP does not suffer from basis set superposition error.⁴⁰

A minimal parameter implicit solvent model has recently been developed within ONETEP.^{10,41} In this model the total potential of the solute is obtained by solving the nonhomogeneous Poisson equation within the self-consistent calculation in ONETEP:

$$\nabla \cdot (\epsilon[\rho] \nabla \phi) = -4\pi\rho_{\text{tot}}(\mathbf{r}), \quad (8)$$

where $\rho_{\text{tot}}(\mathbf{r})$ is the total charge density and is calculated as a sum of the electronic density $\rho(\mathbf{r})$ and the density of the atomic cores. The solute cavity is constructed directly from the electronic density of the solute, which reduces the number of parameters required to only two.⁴² The model includes a smooth transition of the relative permittivity according to the following expression:

$$\epsilon(\mathbf{r}) = 1 + \frac{\epsilon_{\infty} - 1}{2} \left(1 + \frac{1 - (\rho(\mathbf{r})/\rho_0)^{2\beta}}{1 + (\rho(\mathbf{r})/\rho_0)^{2\beta}} \right), \quad (9)$$

where ϵ_{∞} is the bulk permittivity, β controls the smoothness of the transition of $\epsilon(\mathbf{r})$ from 1 to ϵ_{∞} , and ρ_0 is the density value for which the permittivity drops to half that of the bulk. This model was validated on two test sets, one of 60 small molecules (20 neutral, 20 cationic, and 20 anionic) and the second of 71 larger molecules, on which the solvation energies obtained had a root mean square (rms) error with respect to experiment of 3.8 kcal/mol, while the PCM model⁴³ showed an rms error of 10.9 kcal/mol and the highly parameterized state-of-the-art SMD model⁴⁴ had an rms error of 3.4 kcal/mol.

Simulation details

The lysozyme structure was protonated with the MOE⁴⁵ program. MM simulations were carried out using the amber10⁴⁶ package, with the ff99SB⁴⁷ force field used for the protein and the generalized amber

force field (GAFF)⁴⁸ used to model the ligands. Ligand charges were calculated with the AM1-BCC method with antechamber (part of AMBER). The system was explicitly solvated in the TIP3P water model⁴⁹ and the charge neutralized by Cl^- ions.

Since the binding modes of the ligands are all very similar, only catechol bound in the pocket (PDB: 1XEP) was equilibrated. All other ligands were mutated from the catechol at the end point of the equilibration. The system was equilibrated using the following protocol. Hydrogen atoms were relaxed with restraints placed on all heavy atoms in the complex and solvent, before relaxing the solvent with restraints only on the complex. The system was heated to 300 K over 200 ps, still restraining the heavy atoms of the complex, in the NVT ensemble, then run for a further 200 ps with the NPT ensemble at 300 K in order to equilibrate the solvent density. This was cooled over 100 ps to 100 K and a number of relaxations were run, reducing the restraints on the heavy atoms in stages (1000 kcal/mol \AA^{-2} , 500 kcal/mol \AA^{-2} , 100 kcal/mol \AA^{-2} , 50 kcal/mol \AA^{-2} , 20 kcal/mol \AA^{-2} , 10 kcal/mol \AA^{-2} , 5 kcal/mol \AA^{-2} , 2 kcal/mol \AA^{-2} , 1 kcal/mol \AA^{-2} , and 0.5 kcal/mol \AA^{-2}). Finally the system was reheated to 300 K with no restraints over 200 ps and then for a further 200 ps at 300 K in the NPT ensemble to equilibrate the pressure at 1 atm. At this stage, it was confirmed that the water density in the box and the protein structure were stable, as measured by the root mean squared deviation of the protein backbone atoms (converged to 0.8 \AA relative to the initial configuration).

Production simulations were run for 20 ns in the NVT ensemble at 300 K, with the first 1 ns being considered as further equilibration of the ligand in the pocket. All MD simulations used the Langevin thermostat,⁵⁰ the particle mesh Ewald (PME) sum for the treatment of the electrostatics and the SHAKE algorithm⁵¹ to constrain hydrogen-containing bonds, allowing a time-step of 2 fs. For the MM-PBSA calculation an infinite nonbonded cutoff was used with a dielectric constant of 80 to represent the water solvent. The 1-phenylsemicarbazide ligand was treated slightly differently. Since it is significantly bigger than catechol, this ligand was built into the protein pocket using the structure of the benzyl acetate complex with L99A/M102Q double mutant of T4 lysozyme (PDB:3HUK), which is structurally similar to 1-phenylsemicarbazide. This structure was then equilibrated in the same way as catechol, followed by a 20-ns NVT production simulation, the last 19 ns of which were used to generate the snapshots for this study.

In the ONETEP calculations, four NGWFs were used to describe carbon, oxygen, and nitrogen atoms, one NGWF for hydrogen atoms and nine NGWFs for the halogen atoms, all with radii of 8 a_0 . A kinetic energy cutoff of 827 eV for the psinc basis set was used, with the GGA exchange-correlation functional PBE⁵² combined with our implementation of the DFT+D approach

Table I

Total Energies and Binding Energies From ONETEP for Two Snapshots (A and B) of Phenol Bound in the Cavity of T4 Lysozyme L99A/M102Q, and the SCF Convergence Errors of the Calculations

Snapshot	Complex	Receptor	Ligand	Binding energy
A	-7360884.3 ± 0.03	-7326972.6 ± 0.03	-33886.6 ± 0.000005	-25.1
B	-7360982.7 ± 0.07	-7327066.1 ± 0.07	-33886.8 ± 0.000005	-29.8

Energies are given in kcal/mol.

to account for dispersion, parameterized specifically for this functional.³⁴ These settings for our ONETEP calculations were previously compared against calculations with large near-complete Gaussian basis sets and shown to agree with them to less than 0.02 kcal/mol.⁵³ The numerical parameters for QM implicit solvation model were chosen after validation using this protein in a previous study⁹; these are a dielectric constant of 78.54 to represent the water solvent, a β value of 1.3, and numerical parameters for the smeared ion width of $0.8 a_0$ and a discretization order of 8.

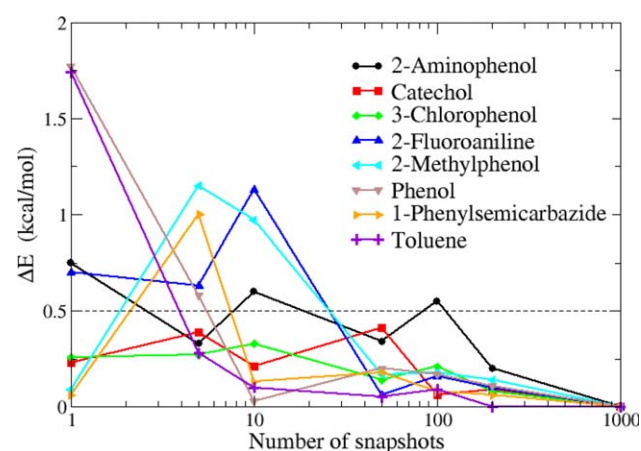
The change in entropy was computed with normal mode analysis in amber10. The structural optimizations were performed first with the conjugate gradients method, followed by the Newton-Raphson method, with very small force tolerances for tight convergence. These were done in the presence of an implicit solvent using the Generalized Born model.

It is important to note that the QM total energies of the complex and host are of the order of millions of kcal/mol, in contrast the binding energies are only a few tens of kcal/mol, a minute value in comparison. Thus, for the accurate calculation of the binding energies the total energies have to be very well converged, and for systems of this size (2600+ atoms) this can be challenging. We examined the convergence of the total energy on one of our large systems (phenol bound in the cavity of T4 lysozyme L99A/M102Q) to ensure that the energies are converged sufficiently well for the calculation of binding energies. The results for two snapshots of phenol bound in the pocket are displayed in Table I. For our test calculations on this system with ONETEP we see very good convergence with errors less than 0.1 kcal/mol.

Snapshots were extracted at constant time intervals from the production trajectory. For MM-PBSA the binding free energies were calculated with an increasing number of snapshots up to a total of 1000 snapshots taken from the 19 ns production simulations. Figure 1 displays the convergence of the MM-PBSA free energies as more snapshots are included in the ensemble, considering the value at 1000 snapshots as the fully converged (standard errors below 0.08 kcal/mol). The maximum error observed using 5 snapshots is 1.15 kcal/mol, for the 2-methylphenol ligand. By using 50 snapshots the maximum error is reduced to less than 0.5 kcal/mol (with catechol having the largest error of 0.41 kcal/mol). Assuming the conver-

gence pattern for the QM calculations is similar, and taking into account the increased computational cost of the QM calculations, in this study we have chosen to use 50 snapshots to calculate the QM-PBSA energies. We can further support the assumption of similar convergence rates if we examine the standard errors for the 50 snapshots for the MM and QM binding energies (both in solvent). For the case of phenol the MM standard error over 50 snapshots is 0.34 kcal/mol (and 0.34 kcal/mol in solvent), while the QM value is 0.35 kcal/mol (0.42 kcal/mol). For catechol the MM error is 0.34 kcal/mol (0.27 kcal/mol) compared to a QM value of 0.38 kcal/mol (0.42 kcal/mol), and for toluene the MM standard error is 0.22 kcal/mol (0.27 kcal/mol) compared to a QM value of 0.24 kcal/mol (0.34 kcal/mol). Thus, MM and QM standard error values are very similar, supporting the assumption that the QM binding energies converge at a similar rate as the MM binding energies shown in Figure 1.

Another issue for the T4 lysozyme L99A/M102Q is that of Val111 in the binding pocket, which is known to have two rotamers with a χ_1 angle of $\sim 180^\circ$ and $\sim -60^\circ$. Studies have shown that using the wrong rotamer can have an effect of up to 4 kcal/mol on the calculated

**Figure 1**

Absolute deviations of the binding energies of the studied ligands as a function of the number of snapshots included in the MM-PBSA calculation, taking 1000 snapshots as the converged value. [Color figure can be viewed in the online issue, which is available at wileyonlinelibrary.com.]

Table II
Ligands Chosen for Study in the T4 Lysozyme Double Mutant L99A/M102Q

L99A/M102Q ligands	ΔG_{exp}	Structure
Toluene	-5.2 [11]	
Phenol	-5.5 [11]	
Catechol	-4.4 [22]	
2-Fluoroaniline	-5.5 [11]	
2-Methylphenol	-4.4 [11]	
3-Chlorophenol	-5.8 [11]	
2-Aminophenol	Nonbinder [21]	
1-Phenylsemicarbazide	Nonbinder [22]	

Experimentally measured free energies of binding (ΔG_{exp}) are given in kcal/mol.

binding free energies.^{14,19} Explicit modeling of this effect has been shown to improve the agreement with experimental binding free energies.¹⁹ We confirmed that our simulations sampled both of these rotamers.

When relative binding free energies are calculated, an approximation that can be used, if ligands are of a similar size and shape, is that the changes in entropy of binding between different ligands are comparable and will cancel each other. To investigate the effect of this approximation for this system, we have also approximated the entropy using normal mode analysis in amber and the results with and without entropy are shown. In Table III, the entropy is calculated as the average from the 50 snapshots taken at constant time intervals from the trajectories.

Ligand hydration energies were calculated using the SMD model⁴⁴ in the Gaussian03 program³⁰ at the M05-2X/6-31G(d) SCRF(IEFPCM, Solvent = Water, SMD) level on a single geometry optimized structure.

RESULTS AND DISCUSSION

We computed the binding free energy of the 8 ligands shown in Table II to the T4 lysozyme double mutant L99A/M102Q using MM-PBSA and QM-PBSA. These ligands were chosen as they comprise of a variety of

chemical and physical properties (polarity, inclusion of halides, size, and binder/nonbinder).

For a protein like this with a buried binding pocket which contains solvent, both the QM and MM models will provide a qualitatively wrong description for the host by adding rather than subtracting the nonpolar contribution of the cavity, as depicted in Figure 2.

We can correct the error described in Figure 2 if we subtract twice the difference between the host and complex nonpolar terms from the host nonpolar solvation energy; once to remove the presence of the erroneous addition of the cavity (making it equal to the description of the complex), and a second time to create a solvent filled cavity. With the observation that the surface tension term used in the QM model takes into account the solute-solvent dispersion and repulsion,¹⁰ we wish to remove only the spurious cavitation from our model of the host, whilst leaving the physically correct dispersion-repulsion contributions. The corrected host solvation energy is then given by Equation 12.

$$\Delta \text{SASA} = \text{SASA}_{\text{host}} - \text{SASA}_{\text{complex}}$$

$$E_{\text{cav}} = \gamma \cdot \text{SASA}$$

$$E_{\text{dis-rep}} = -\gamma' \cdot \text{SASA}$$

$$E_{\text{non-polar}} = E_{\text{cav}} + E_{\text{disp-rep}} = (\gamma - \gamma') \cdot \text{SASA} = \tilde{\gamma} \cdot \text{SASA}.$$

$$\Delta \text{SASA} = \frac{1}{\tilde{\gamma}} \left(E_{\text{non-polar}}^{\text{host}} - E_{\text{non-polar}}^{\text{complex}} \right).$$

(10)

$$E_{\text{cav-corr}}^{\text{QM}} = 2\gamma \cdot \Delta \text{SASA} = 2\frac{\gamma}{\tilde{\gamma}} \left(E_{\text{non-polar}}^{\text{host}} - E_{\text{non-polar}}^{\text{complex}} \right)$$

(11)

$$\simeq 7.116 \left(E_{\text{non-polar}}^{\text{host}} - E_{\text{non-polar}}^{\text{complex}} \right).$$

$$\Delta E_{\text{host-solvation}}^{\text{QM}} = E_{\text{host-solv}}^{\text{QM}} - E_{\text{cav-corr}}^{\text{QM}} - E_{\text{host-vac}}^{\text{QM}}.$$

(12)

Here γ is the solvent surface tension, while γ' is an additional factor to γ that introduces dispersion-repulsion interactions, SASA is the solvent-accessible surface area, E_{cav} is the cavitation energy, $E_{\text{dis-rep}}$ is the solute-solvent dispersion-repulsion energy, $E_{\text{non-polar}}^{\text{host}}$ is the total nonpolar solvation energy, and $E_{\text{cav-corr}}^{\text{QM}}$ is the QM correction to the cavitation energy. This is also the case with the MM nonpolar energy, with the buried pocket adding to the surface area, causing the host to have a larger cavitation energy than the complex. We have treated the MM in a similar way, subtracting twice the difference of the host and complex nonpolar energy:

$$E_{\text{cav-corr}}^{\text{MM}} = 2 \cdot \left(E_{\text{non-polar}}^{\text{host}} - E_{\text{non-polar}}^{\text{complex}} \right).$$

(13)

$$\Delta E_{\text{host-solvation}}^{\text{MM}} = E_{\text{host-solv}}^{\text{MM}} - E_{\text{cav-corr}}^{\text{MM}} - E_{\text{host-vac}}^{\text{MM}}.$$

Table III presents the computed binding free energies of these ligands (relative to phenol which is normalized

Table III

QM-PBSA (Top) and MM-PBSA (Bottom) Binding Free Energies for 50 Snapshots Relative to Phenol

Ligand	$\Delta G_{\text{bind,vac}}^{\text{QM}}$	$\Delta G_{\text{bind,solv}}^{\text{QM}}$	$\Delta G_{\text{bind,solv}}^{\text{QM}} - T\Delta S$	ΔG^{exp}
Catechol	-13.9 ± 0.38	-9.0 ± 0.42	-8.6 ± 0.67	-4.4 [22]
3-Chlorophenol	-8.1 ± 0.26	-6.9 ± 0.40	-7.7 ± 0.67	-5.8 [11]
2-Fluoroaniline	-4.3 ± 0.25	-5.9 ± 0.42	-4.8 ± 0.55	-5.5 [11]
2-Methylphenol	-8.2 ± 0.25	-8.5 ± 0.37	-7.0 ± 0.61	-4.4 [11]
Toluene	1.6 ± 0.24	-4.8 ± 0.35	-4.4 ± 0.59	-5.2 [11]
1-Phenylsemicarbazide	-19.8 ± 0.49	-0.3 ± 0.55	3.8 ± 0.70	Nonbinder [22]
2-Aminophenol	-12.2 ± 0.41	-6.2 ± 0.39	-5.1 ± 0.51	Nonbinder [21]
Phenol (reference)	-5.6 ± 0.35	-5.6 ± 0.42	-5.6 ± 0.59	-5.6 [11]
Max error ^a	19.8	6.2	5.1	
RMS error	10.0	3.3	2.7	
Catechol	-16.0 ± 0.34	-4.1 ± 0.27	-3.7 ± 0.60	-4.4 [22]
3-Chlorophenol	-9.6 ± 0.25	-8.8 ± 0.27	-9.2 ± 0.73	-5.8 [11]
2-Fluoroaniline	-5.7 ± 0.28	-8.5 ± 0.33	-7.4 ± 0.46	-5.5 [11]
2-Methylphenol	-8.2 ± 0.27	-7.2 ± 0.23	-6.1 ± 0.61	-4.4 [11]
Toluene	0.8 ± 0.22	-7.5 ± 0.27	-7.1 ± 0.50	-5.2 [11]
1-Phenylsemicarbazide	-22.9 ± 0.42	-11.6 ± 0.37	-7.5 ± 0.55	Nonbinder [22]
2-Aminophenol	-13.2 ± 0.40	-7.1 ± 0.39	-6.1 ± 0.50	Nonbinder [21]
Phenol (reference)	-5.6 ± 0.34	-5.6 ± 0.34	-5.6 ± 0.49	-5.6 [11]
Max error ^a	22.9	11.6	7.5	
RMS error	11.3	5.5	4.0	

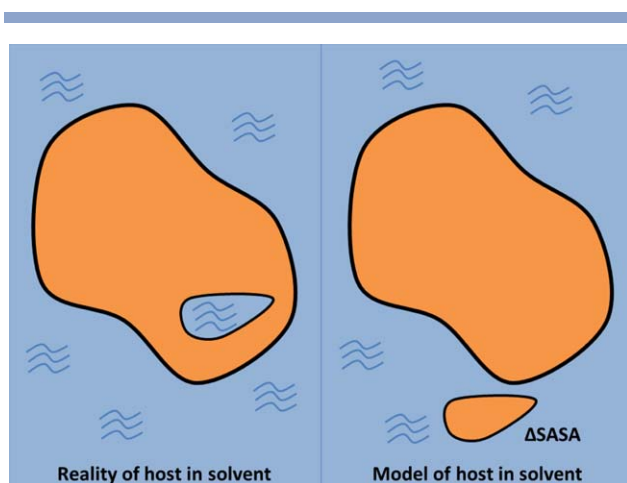
Standard errors for each ligand are included as obtained from the binding energies of the 50 snapshots. All energies in kcal/mol.

^aThe experimental binding energy for the nonbinders is set to 0.00 kcal/mol, unless the prediction is positive, in which case the error is assumed 0.00 kcal/mol.

to the experimental binding free energy of phenol to T4 lysozyme double mutant L99A/M102Q), averaged over 50 snapshots. The top table shows the QM binding energies in vacuum, solvent, and with entropic contributions calculated from normal mode analysis (from the MM

calculations), alongside the experimentally obtained values. The lower table displays the same data obtained from MM-PBSA.

Looking at the MM binding free energies (averaged over 50 snapshots) in Table III, we observe that the relative binding free energies from MM-PBSA are not very close to the experimental values. There are two exceptions, catechol that has a calculated relative binding free energy with an error of 0.7 kcal/mol when compared to the experimental value, and 2-methylphenol which has an error of 0.9 kcal/mol from experiment. The smallest error for the other binding ligands is almost 2 kcal/mol. The binding free energies from QM-PBSA are improved, with two ligands having errors less than 0.8 kcal/mol from experiment (2-fluoroaniline and toluene). Catechol, in contrast to MM-PBSA, has the largest error (with respect to the experimental value) of the known binders overestimated by 4.1 kcal/mol. Given that the vacuum binding energies from MM and QM correlate very well, as we can observe in Table III, the difference observed in the binding energies in solvent is primarily due to the solvation energies. For a deeper understanding, we will look at only the solvation energy of the ligands. We will use catechol as an example, since the MM-PBSA relative binding free energy is very close to the experimental value whilst the QM-PBSA value is not. The experimental hydration free energy of catechol is -9.4 kcal/mol.⁵⁴ The QM hydration free energy averaged over the 50 snapshots is -8.1 kcal/mol. In contrast, the MM

**Figure 2**

Left: The host in reality. Right: The host as described by the solvation model, in terms of its contributions to the cavitation energy. In the model, the surface area of the buried pocket is added to the cavitation energy contribution of the host, providing a qualitatively wrong description of the host. ΔSASA is the difference in the solvent accessible surface area between the complex and host. [Color figure can be viewed in the online issue, which is available at wileyonlinelibrary.com.]

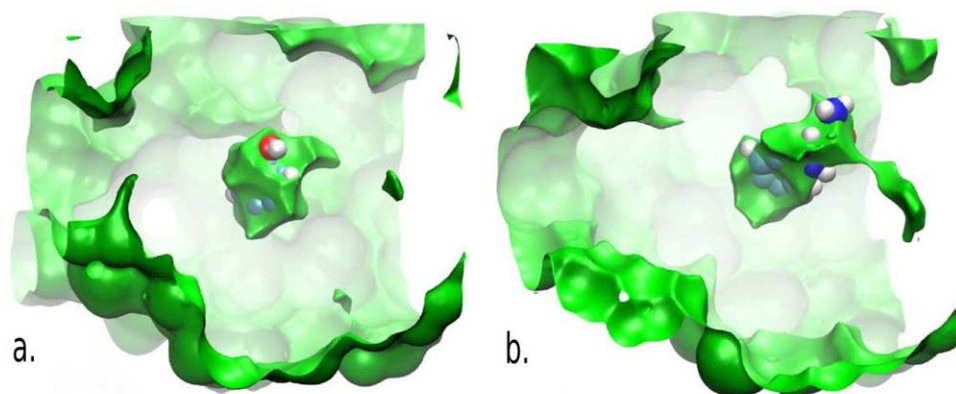


Figure 3

The dielectric permittivity from QM calculations at an isovalue of 70 inside of the host, extracted from the complex geometry, with (a) phenol bound, and (b) phenylsemicarbazide bound. The ligands have been superimposed as a guide to the eye. The ligand-containing green volumes in the middle are the cavities that contribute to the solvation energy, while the apparently empty space is occupied by the protein.

hydration free energy averaged over the same 50 snapshots, is -20.9 kcal/mol. This shows that the MM hydration energy is substantially overestimated; however MM-PBSA still produces a very good relative binding free energy compared to experiment. Since MM and QM binding energies in vacuum are so close to each other, this suggests that both MM and QM overbind the catechol in the pocket in vacuum, however the excessively large solvation energy from MM-PBSA cancels out the overbinding in vacuum to give a final relative free energy of binding that does agree closely with experiment.

MM-PBSA predicts 1-phenylsemicarbazide, which is an experimental nonbinder, to be a strong binder, while QM-PBSA correctly predicts that this molecule is a nonbinder. This is a consequence of the much larger size of this ligand and the contributions this makes to the solvation energy in each model. 1-Phenylsemicarbazide has the largest binding energy in vacuum for both MM and QM descriptions. Due to the larger size, 1-phenylsemicarbazide also shows more pronounced changes in the entropy of binding, which results in a difference of around 4.1 kcal/mol in the calculated binding entropy compared to phenol. Thus, the approximation of entropy cancellation is not valid in this case and indeed the inclusion of entropy has a large effect for both the MM-PBSA and QM-PBSA results for this ligand. We can assess the increase in the binding pocket volume in the case of 1-phenylsemicarbazide by examining Figure 3, which displays the dielectric permittivity from the quantum solvation model within the binding pocket at an isovalue of 70, for the host as extracted from the complex geometry with phenol bound (3.a) or with 1-phenylsemicarbazide bound (3.b). This clearly shows the enlargement of the cavity caused by the presence of the larger ligand. Solvation energies are also very important. The desolvation energy of this ligand is larger than the

others due to its large polar chain and the solvation energy of the host is also increased compared to the host solvation energies for the other ligands due to the enlarged cavity, so both of these effects act to destabilize the binding of 1-phenylsemicarbazide. The combination of these effects as shown in Table III produces a positive free energy of binding showing that this ligand is a nonbinder for the QM calculations, while it is still predicted to be a strong binder by the MM calculations. As the geometries are the same between the MM and QM calculations and also the relative energies in vacuum agree closely (around 3 kcal/mol), we conclude that the more rigorous QM solvation model is responsible for producing the correct result for this case. This deciding role of the solvent is also demonstrated by previous calculations using the more thermodynamically rigorous TI technique in explicit solvent in which case 1-phenylsemicarbazide was also predicted to be a nonbinder.²²

It is interesting to observe that 2-aminophenol which is a known decoy,²¹ that is, an experimental nonbinder that computational approaches predict as a binder, lives up to its name and is predicted to be a good binder by both the MM and QM techniques in our study. By examining the binding energies in vacuum we observe that 2-aminophenol, as is the case with catechol, has very large binding energies (-12.2 kcal/mol for QM and -13.2 for MM). While this is to be expected as the amine and hydroxyl groups can each form a hydrogen bond in the cavity while most other ligands form a single hydrogen bond, the computed binding energies appear to be larger than we might expect, even for a bidentate ligand. Graves *et al.*²¹ also suggest that both catechol and 2-aminophenol are expected to share the same binding modes within the cavity. They attribute the lack of binding for 2-aminophenol to an expectation that it should have a larger desolvation energy than catechol due to the

Table IV

Comparison of QM-PBSA and MM-PBSA Ligand Absolute (Top) and Relative (Bottom) Hydration Energies With Experimental Hydration Energies

Molecule	$\Delta G_{\text{lig, solv}}^{\text{SMD}}$	$\Delta G_{\text{lig, solv}}^{\text{exp}}$	$\Delta G_{\text{lig, solv}}^{\text{MM}}$	$\Delta G_{\text{lig, solv}}^{\text{QM}}$
Catechol	-9.3	-9.4 [54]	-20.9	-8.1
3-Chlorophenol	-6.7	-	-9.9	-3.6
2-Fluoroaniline	-4.5	-	-5.4	-3.2
2-Aminophenol	-9.8	-	-13.9	-8.0
2-Methylphenol	-6.3	-5.9 [55]	-9.0	-2.9
1-Phenylsemicarbazide	-15.1	-	-16.2	-13.8
Toluene	-1.3	-0.9 [55]	-1.4	1.4
Phenol	-6.7	-6.6 [55]	-9.7	-3.7
Relative hydration energies				
Catechol	-2.5	-2.8	-11.1	-4.3
3-Chlorophenol	0.1	-	-0.1	0.1
2-Fluoroaniline	2.3	-	4.4	0.6
2-Aminophenol	-3.1	-	-4.1	-4.2
2-Methylphenol	0.4	0.7	0.8	0.9
1-Phenylsemicarbazide	-8.4	-	-6.4	-10.1
Toluene	5.4	5.7	8.3	5.1
Phenol (reference)	0.0	0.0	0.0	0.0
Max error ^a			8.6	1.8
RMS error ^a			3.4	1.2

Hydration energies averaged over the 50 chosen snapshots (energies in kcal/mol).

^aError calculation used SMD values as reference.

perceived ability of the amine to stabilize more hydrogen bonds in water. This is not confirmed however from our ligand hydration energies as calculated with three different solvation models. For example, the most accurate hydration free energy values we can obtain from the QM models, for catechol and 2-aminophenol differ by 0.5 kcal/mol for the SMD model and 0.1 kcal/mol for our model. Therefore the experimental result, which has been obtained by the thermal upshift denaturation temperature technique, may need to be checked with more accurate methods. While the MM solvation energy of 2-aminophenol is overestimated by about 4 kcal/mol, this is not as large as the 12 kcal/mol overestimation of the catechol MM solvation energy, and does not cause the same fortuitous error cancellation that led to the remarkable agreement with experiment for the MM binding free energy of catechol. If we did have the same level of error in the MM solvation energy of 2-aminophenol, MM-PBSA would predict it as essentially a nonbinder.

If we exclude 1-phenylsemicarbazide for the reasons we have already discussed, all other ligands have entropies of binding much closer to phenol, between 0.4 kcal/mol and 1.6 kcal/mol, with the largest value being for 2-methylphenol. Although this difference in entropies is quite small, we do observe an overall improvement in the agreement with experiment when entropy is included in the calculation of the relative binding free energies averaged over 50 snapshots for all ligands, for both MM-PBSA and QM-PBSA. Therefore the argument that entropies of binding for ligands of similar size can be ignored when calculating relative free energies of binding is par-

tially valid and could be applied in cases where the calculation of vibrational entropies is not feasible. In the case of 1-phenylsemicarbazide, which is much larger and more flexible than the other ligands, the effect of the entropy is significant and cannot be ignored. A more rigorous theoretical approach for including entropy in the calculation of free energies of binding is TI. However, even with MM calculations, this approach is computationally extremely demanding compared to MM-PBSA as it requires explicit solvent and multiple MD simulations “mutating” one ligand to another. Boyce *et al.*²² have used MM-based TI simulations to calculate free energies of binding of 8 ligands to the same protein as we. Their ligands are small rigid aromatic molecules and they have in common with us the ligands catechol, phenol and 2-methylphenol. Their rms errors of the relative binding free energies from phenol to their other ligands with respect to experimentally measured values (obtained from ITC) were 2.5 kcal/mol, and using catechol as a reference, 1.1 kcal/mol. Our QM-PBSA calculations have comparable rms error of 2.7 kcal/mol while MM-PBSA has a larger rms error of 4.0 kcal/mol. These comparisons make it clear that the rigorous calculation of the entropy of binding is equally important to the accurate description of the intermolecular interactions that the QM method provides.

We have already discussed the effect of the solvation model, which plays a major role in the free energies of binding that each method provides. More in depth information can be obtained from Table IV where we present all the ligand hydration energies that we have available. The experimentally obtained hydration energies of catechol, 2-methylphenol, phenol and toluene are -9.4 kcal/mol,⁵⁴ -5.9 kcal/mol,⁵⁵ -6.6 kcal/mol,⁵⁵ and -0.9 kcal/mol,⁵⁵ respectively. Hydration energies obtained from QM-PBSA averaged over 50 snapshots are -8.1 kcal/mol, -2.9 kcal/mol, -3.7 kcal/mol, and 1.4 kcal/mol in contrast to MM-PBSA which gives -20.9 kcal/mol, -9.0 kcal/mol, -9.8 kcal/mol, and -1.5 kcal/mol. Table IV shows also the hydration energies of all the ligands as calculated with the SMD model as well. We can clearly see that the MM-PBSA hydration energies are less accurate and this impacts the outcome of the free energy calculations. The QM-PBSA energies on the other hand have a smaller error and the relative hydration energies are substantially closer to experimentally obtained values. For the classical solvation model, the maximum error for the relative solvation energies of the ligands is 8.6 kcal/mol, with an rms error 2.1 kcal/mol, compared with 1.8 kcal/mol maximum error and 1.2 kcal/mol rms error for our QM solvation model. The more accurate QM solvation energies result in improved binding free energies for the majority of the ligands.

Finally, it is interesting to consider the computational effort required for our QM-PBSA calculations. As would be expected, even with a linear scaling and highly parallelized DFT program such as ONETEP, these calculations

are significantly more computationally expensive than the MM calculations. A single QM-PBSA energy evaluation (i.e., achieving self-consistent convergence in implicit solvent) on a representative complex structure (2615 atoms) took approximately 28 h on 48 Intel[®] Xeon[®] E5-2670 processor cores. This is around 4.8×10^7 core-seconds, compared to the MM-PBSA energy evaluation on the same structure that took just 11 s on one (slightly slower) Intel[®] Xeon[®] E5-2650 processor core. Even with the small difference in core speeds taken into account, the QM-PBSA energy evaluation is about six orders of magnitude more computationally demanding than MM-PBSA. However, the point is that with linear-scaling DFT approaches, run on modest computational resources which are widely available today, free energy calculations on entire proteins encompassing thousands of atoms are becoming feasible. While the computational effort is and will remain much higher than MM-based approaches, the ability to run full DFT calculations on thousands of atoms with a near-complete basis set obtaining superior accuracy and transferability compared to MM, means that such calculations are likely to become a useful tool in drug optimization.

CONCLUSIONS

We have developed a QM-PBSA approach for the calculation of free energies of binding, in which large-scale DFT calculations with a near-complete basis set are performed to evaluate the energy of the configurations in place of the force field that is used in the conventional MM-PBSA technique. The solvation effects in the DFT calculations are described by a minimal parameter self-consistent implicit solvent model. We applied this QM-PBSA approach to compute the relative binding free energies of eight small aromatic ligands bound in the polar cavity of the T4 lysozyme mutant L99A/M102Q protein which contains 2601 atoms, and have compared our results to the traditional MM-PBSA method. To our knowledge, this is the first study where an entire protein–ligand system is described by a DFT approach with a self-consistent implicit solvent model.

All the structures were obtained from classical molecular dynamics simulations. The free energy calculations have been converged to within 0.5 kcal/mol with respect to the number of snapshots included in the ensembles for both the MM and QM approaches. Our aim was to explicitly account for electronic polarization and charge transfer via the DFT calculations. We observed remarkable agreement between the MM and QM binding energies in vacuum, which indicates that the parametrization of the force field in this case is good enough to capture, in an average way, effects of polarization and charge transfer for the T4 lysozyme mutant L99A/M102Q. With the QM and MM vacuum energies agreeing so closely,

the differences in the final binding free energies are due to the solvation energies. Thus, we observe significant differences when computing free energies of binding in solvent and we have found that our DFT-based solvation model is overall more consistent and accurate than the MM model. For the eight ligands we used in this study the rms error in free energies of binding is 4.0 kcal/mol for MM-PBSA, whereas QM-PBSA reduces this error to 2.7 kcal/mol. This demonstrates that at least the solvent-induced polarization needs to be treated explicitly in order to improve the reliability of such free energy approaches.

Even though the QM-PBSA results are overall more accurate, the approach performs significantly worse for the catechol ligand. MM-PBSA's improved accuracy for this ligand in particular appears to be fortuitous error cancellation between overbinding in vacuum and a ligand hydration energy that is over twice the experimental value. It is important to note that the ligands in our set contain two nonbinders that MM-PBSA predicts as good binders, whereas QM-PBSA correctly predicts one of these as a nonbinder.

The T4 lysozyme double mutant is a challenging system, as not only do all the experimentally confirmed binders in our study have very similar binding free energies but also the buried cavity is a challenge for the implicit solvation models. In addition to this, the advantage of explicitly accounting for the electrons is offset by the simplicity of the protein and ligands we have used here, which, as we have shown are described very well by the force field. Although the sample size of this study was small, our full QM-PBSA approach has given very encouraging results. We expect that QM-PBSA simulations of this kind will prove beneficial in future computational drug optimization studies, especially in cases where the ligands have functional groups whose interactions with the hosts are not captured accurately by available force fields and their parametrizations.

ACKNOWLEDGMENTS

SJF thanks the BBSRC and Boehringer Ingelheim for an industrial CASE studentship. C-KS thanks the Royal Society for a University Research Fellowship. The authors thank the University of Southampton for the Iridis3 and Iridis4 supercomputers that were used in this work.

REFERENCES

1. Gilson MK, Zhou H-X. Calculation of protein-ligand binding affinities. *Annu Rev Biophys Biomol Struct* 2007;36:21-42.
2. Brandsdal BO, Österberg F, Almlöf M, Feierberg I, Luzhkov VB, Åqvist J. Free energy calculations and ligand binding. *Adv Protein Chem* 2003;66:123-158.
3. Zwanzig R. High-temperature equation of state by a perturbation method. I. nonpolar gases. *J Chem Phys* 1954;22:1420-1426.
4. Christ CD, Mark AE, van Gunsteren WF. Basic ingredients of free energy calculations: A review. *J Comp Chem* 2010;31:1569-1582.

5. Kirkwood JG. Statistical mechanics of fluid mixtures. *J Chem Phys* 1935;3:300-313.
6. Halperin I, Ma BY, Wolfson H, Nussinov R. Principles of docking: An overview of search algorithms and a guide to scoring functions. *Proteins* 2002;47:409-443.
7. Srinivasan J, Cheatham TE, Cieplak P, Kollman PA, Case DA. Continuum solvent studies of the stability of DNA, RNA, and phosphoramidate-DNA helices. *J Am Chem Soc* 1998;120:9401-9409.
8. Skylaris C-K, Haynes PD, Mostofi AA, Payne MC. Introducing {ONETEP}: Linear-scaling density functional simulations on parallel computers. *J Chem Phys* 2005;122:084119.
9. Dziedzic J, Fox SJ, Fox T, Tautermann C, Skylaris C-K. Large-scale {DFT} calculations in implicit solvent - {A} case study on the {T}4 lysozyme {L}99{A}/{M}102{Q} protein. *Int J Quantum Chem* 2012; 113:771-785.
10. Dziedzic J, Helal HH, Skylaris C-K, Mostofi AA, Payne MC. Minimal parameter implicit solvent model for ab initio electronic structure calculations. *Europhys Lett* 2011;95:43001.
11. Wei BQ, Baase WA, Weaver LH, Matthews BW, Shoichet BK. A model binding site for testing scoring functions in molecular docking. *J Mol Biol* 2002;322:339-355.
12. Baase WA, Zhang XJ, Heinz DW, Blaber M, Baldwin EP, Matthews BW, Eriksson AE. Response of a protein-structure to cavity-creating mutations and its relation to the hydrophobic effect. *Science* 1992; 255:178-183.
13. Eriksson AE, Baase WA, Matthews BW. Similar hydrophobic replacement of Leu99 and Phe153 within the core of T4-lysozyme have different structural and thermodynamic consequences. *J Mol Biol* 1993;229:747-769.
14. Deng Y, Roux B. Calculation of standard binding free energies: Aromatic molecules in the {T}4 lysozyme {L99A} mutant. *J Chem Theory Comput* 2006;2:1255-1273.
15. Morton A, Baase W, Matthews BW. Energetic origins of specificity of ligand binding in an interior nonpolar cavity of {T}4 {L}ysozyme. *Biochemistry* 1995;34:8564-8575.
16. Morton A. Specificity of ligand binding in a buried nonpolar cavity of {T}4 lysozyme: Linkage of dynamics and structural plasticity. *Biochemistry* 1995;34:8576-8588.
17. Gallicchio E, Lapelosa M, Levy RM. Binding energy distribution analysis method ({BEDAM}) for estimation of protein-Ligand binding affinities. *J Chem Theory Comput* 2010;6:2961-2977.
18. Leitgeb M, Karplus M, Boresch S, Tettering F. Absolute binding free energies: A quantitative approach for their calculation. *J Phys Chem B* 2003;107:9535-9551.
19. Mobley DL, Graves AP, Chodera JD, McReynolds AC, Shoichet BK, Dill KA. Predicting absolute ligand binding free energies to a simple model site. *J Mol Biol* 2007;371:1118-1134.
20. Deng Y, Roux B. Computations of standard binding free energies with molecular dynamics simulations. *J Phys Chem B* 2009;113: 2234-2246.
21. Graves AP, Brenk R, Shoichet BK. Decoys for docking. *J Med Chem* 2005;48:3714-3728.
22. Boyce SE, Mobley DL, Rocklin GJ, Graves AP, Dill KA, Shoichet BK. Predicting ligand binding affinity with alchemical free energy methods in a polar model binding site. *J Mol Biol* 2009;394:747-763.
23. Graves AP, Shivakumar DM, Boyce SE, Jacobson MP, Case DA, Shoichet BK. Rescoring docking hit lists for model cavity sites: Predictions and experimental testing. *J Mol Biol* 2008;377:914-934.
24. Massova I, Kollman PA. Computational alanine scanning to probe protein-protein interactions: A novel approach to evaluate binding free energies. *J Am Chem Soc* 1999;121:8133-8143.
25. Kaukonen M, Söderhjelm P, Heimdal J, Ryde U. {QM/MM-PBSA} method to estimate free energies for reactions in proteins. *J Phys Chem B* 2008;112:12537-12548.
26. Rod TH, Ryde U. A method for calculating high-level {QM/MM} free energies for enzymatic reactions: methyl transfer catalyzed by catechol {O}-methyltransferase. *Phys Rev Lett* 2005;94:198302.
27. Wang M, Wong CF. Rank-ordering protein-ligand binding affinity by a quantum mechanics/molecular mechanics/Poisson-Boltzmann-surface area model. *J Chem Phys* 2007;126:026101.
28. Soler JM, Artacho E, Gale JD, Garcia A, Junquera J, Ordejon P, Sanchez D. The {S}iesta method for ab initio order-N materials simulation. *J Phys Cond Mater* 2002;14:2745-2779.
29. Davis ME, Madura JD, Luty BA, McCammon JA. Electrostatic and diffusion of molecules in solution: {S}imulations with the University of Houston Brownian Dynamics Program. *Comp Phys Commun* 1991;62:187-197.
30. Frisch MJ, Trucks GW, Schlegel HB, Scuseria GE, Robb MA, Cheeseman JR, Montgomery JJA, Vreven T, Kudin KN, Burant JC, Millam JM, Iyengar SS, Tomasi J, Barone V, Mennucci B, Cossi M, Scalmani G, Rega N, Petersson GA, Nakatsuji H, Hada M, Ehara M, Toyota K, Fukuda R, Hasegawa J, Ishida M, Nakajima T, Honda Y, Kitao O, Nakai H, Klene M, Li X, Knox JE, Hratchian HP, Cross JB, Bakken V, Adamo C, Jaramillo J, Gomperts R, Stratmann RE, Yazyev O, Austin AJ, Cammi R, Pomelli C, Ochterski JW, Ayala PY, Morokuma K, Voth GA, Salvador P, Dannenberg JJ, Zakrzewski VG, Dapprich S, Daniels AD, Strain MC, Farkas O, Malick DK, Rabuck AD, Raghavachari K, Foresman JB, Ortiz JV, Cui Q, Baboul AG, Clifford S, Cioslowski J, Stefanov BB, Liu G, Liashenko A, Piskorz P, Komaromi I, Martin RL, Fox DJ, Keith T, Al-Laham MA, Peng CY, Nanayakkara A, Challacombe M, Gill PMW, Johnson B, Chen W, Wong MW, Gonzalez C, Pople JA. Gaussian 03, revision C.02. Wallingford, CT: Gaussian, Inc.; 2004.
31. Diaz N, Suárez D, Merz KM, Sordo TL. Molecular dynamics simulations of the TEM-1 {β}-lactamase complexed with cephalothin. *J Med Chem* 2005;48:780-791.
32. Dixon SL, van der Vaart A, Wang B, Gogonea V, Vincent JJ, Brothers EN, Suarez D, Westerhoff LM, Merz JKM, Divcon. University Park, PA: The Pennsylvania State University; 2004.
33. Cole DJ, Skylaris C-K, Rajendra E, Venkitaraman AR, Payne MC. Protein-protein interaction from linear-scaling first-principles quantum-mechanical calculations. *Europhys Lett* 2010;91:37004.
34. Hill Q, Skylaris C-K. Including dispersion interactions in the {ONETEP} program for linear-scaling density functional theory calculations. *Proc R Soc A* 2009;465:669-683.
35. Fox S, Wallnoefer HG, Fox T, Tautermann CS, Skylaris C-K. First principles-based calculations of free energy of binding: Application to ligand binding in a self-assembling superstructure. *J Chem Theory Comput* 2011;7:1102-1108.
36. Skylaris C-K, Haynes PD, Mostofi AA, Payne MC. Implementation of linear scaling plane wave density functional theory on parallel computers. *Phys Stat Sol* 2006;243:973-988.
37. Hine NDM, Haynes PD, Mostofi AA, Skylaris C-K, Payne MC. Linear-scaling density-functional theory with tens of thousands of atoms: Expanding the scope and scale of calculations with ONETEP. *Comp Phys Commun* 2009;180:1041-1053.
38. Skylaris C-K, Mostofi AA, Haynes PD, Diéguéz O, Payne MC. Non-orthogonal generalized Wannier function pseudopotential plane-wave method. *Phys Rev B* 2002;66:035119.
39. Mostofi AA, Haynes PD, Skylaris C-K, Payne MC. Preconditioned iterative minimization for linear-scaling electronic structure calculations. *J Chem Phys* 2003;119:8842-8848.
40. Haynes PD, Skylaris C-K, Mostofi AA, Payne MC. Elimination of the basis set superposition error in linear-scaling density-functional calculations with local orbitals optimized in situ. *Chem Phys Lett* 2006;422:345-349.
41. Anton L, Dziedzic J, Skylaris C-K, Probert M. Multigrid solver module for onetep, castep and other codes. <http://www.hector.ac.uk/cse/distributedcse/reports/onetep/>; 2013.

42. Fattebert J-L, Gygi F. Density functional theory for efficient ab initio molecular dynamics simulations in solution. *J Comp Chem* 2002;23:662-666.
43. Tomasi J, Persico M. Molecular interactions in solution: An overview of methods based on continuous distributions of the solvent. *Chem Rev* 1994;94:2027-2094.
44. Marenich AV, Cramer CJ, Truhlar DG. Universal solvation model based on solute electron density and on a continuum model of the solvent defined by the bulk dielectric constant and atomic surface tensions. *J Phys Chem B* 2009;113:6378-6396.
45. Molecular operating environment (MOE), 2013.08. Montreal, QC, Canada: Chemical Computing Group Inc.; 2013.
46. Case DA, Darden T, Cheatham T, Simmerling C, Wang J, Duke R, Luo R, Crowley M, Roitberg SHA, Seabra G, Kolossváry I, Wong KF, Paesani F, Vanicek J, Wu X, Brozell SR, Steinbrecher T, Gohlke H, Yang H, Tan C, Mongan J, Hornak V, Cui G, Mathews D, Seetin M, Sagui C, Babin V, Kollman PA. Amber10; 2008.
47. Hornak V, Abel R, Okur A, Strockbine B, Roitberg A, Simmerling C. Comparison of multiple amber force fields and development of improved protein backbone parameters. *Proteins* 2006;65:712-725.
48. Wang J, Wolf RM, Caldwell JW, Kollman PA, Case DA. Development and testing of a general amber force field. *J Comp Chem* 2004;25:1157-1174.
49. Jorgensen WL, Chandrasekhar J, Madura JD. Comparison of simple potential functions for simulating liquid water. *J Chem Phys* 1983;79:926-935.
50. Alderman SA, Doll JD. Generalized Langevin equation approach for atom-solid-surface scattering - general formulation for classical scattering off harmonic solids. *J Chem Phys* 1976;64:2375-2388.
51. Ryckaert J-P, Ciccotti G, Berendsen HJC. Numerical integration of the cartesian equations of motion of a system with constraints: molecular dynamics of n-alkanes. *J Comput Phys* 1977;23:327-341.
52. Perdew JP, Burke K, Ernzerhof M. Generalized gradient approximation made simple. *Phys Rev Lett* 1996;77:3865-3868.
53. Fox S, Pittock C, Fox T, Tautermann C, Malcolm N, Skylaris C-K. Electrostatic embedding in large-scale first principles quantum mechanical calculations on biomolecules. *J Chem Phys* 2011;135:224107.
54. Mordasini TZ, McCammon JA. Calculations of relative hydration free energies: A comparative study using thermodynamic integration and an extrapolation method based on a single reference state *J Phys Chem B* 2000;104:360-397.
55. Marenich AV, Kelly CP, Thompson JD, Hawkins GD, Chambers CC, Giesen DJ, Winget P, Cramer CJ, Truhlar DG. Minnesota solvation database—version 2012. Minneapolis: University of Minnesota; 2012.